Fog removal in images using improved dark channel prior and contrast limited adaptive histogram equalization

Rajiv Kapoor[1] · Rashmi Gupta[2] · Le Hoang Son[3,4] · Raghvendra Kumar[5] · Sudan Jha[6]

Abstract

It is necessary to perform fog removal from an image based on the estimation of depth to increase the visibility of a scene. In this paper, we propose a new algorithm to eradicate fog from images in which fog is defined as a state or cause of perplexity or confusion with respect to the image. It runs at high speed and simultaneously minimizes the halo-artifact with a new median operator in dark channel prior. The proposed method is based on Guided Filter for transmission-map refinement and Contrast Limited Adaptive Histogram Equalization (CLAHE) for visibility improvement. It preserves small details while remaining robust against density of fog, and recovers scene contrast simultaneously. Guided filter improved the transmission map acquired from Median dark channel prior (MDCP), which is an improvement of the Dark Channel Prior DCP by the use of median operation. All of the parameters used in our method are data driven. The quality of algorithm has been validated on several types of fog-degraded images where considerable variation in contrast and illumination exists. Moreover, its performance is compared with the other state-of-the-art methods. The experimental results indicate that the proposed method effectively restores the color and contrast of scene as well as produces satisfactory information in homogeneous fog. It outperforms the existing fog removal methods for run time computational time and other evaluation metrics for rating of visibility enhancement. The proposed method conserves small details part of the image when outstanding vigorous against concentration of fog, and recuperate scene contrast instantaneously. It controls at a high speed than the existing approaches and can diminish the halo effect.

Keywords Atmospheric dichromatic model · Computer vision · Contrast limited adaptive histogram equalization · Dark channel prior · Defogging · Guided filter

✉ Le Hoang Son
sonlh@vnu.edu.vn

Extended author information available on the last page of the article

1 Introduction

Outdoor scene images may be degraded through various reasons in which the most notable source is bad weather conditions such as haze, smoke and fog [5]. The outdoor surveillance systems effect is obviously limited through fog [18]. Recently, many challenges have been encountered in computer vision and graphics communities to remove fog by using minimal inputs, i.e. a single image [13]. In outdoor environments when images are captured from optical devices, light after reflecting from an object leads to scattering of light in the atmosphere prior to reaching the camera [43]. In the presence of pollutants or atmospheric particles in the air in forms of dust, smoke, fog, rain and snow, these atmospheric particles result in two fundamental phenomena called 'direct distortion' and 'distortion contributed by atmospheric light' [33]. Direct distortion reduces the contrast and atmospheric light distortion adds whiteness in the scene which creates a problem of color ambiguity [21]. As a result, images taken under such conditions are characterized by having poor contrast and visibility [20]. Therefore, elimination of air-light and restoration of contrast is essential for outdoor vision application used for object recognition, tracking and navigation [32].

A reliable visibility restoration method requires accurate estimation of air-light and transmission map [13]. From the past few decades, several methods have been proposed to remove fog using many numbers of images. In [21, 27], the authors removed fog by taking more than two images of the same scenes (e.g. one in dense fog and another in normal fog). However in general scenarios, these strategies are not practical since weather may remain unchanged for several minutes or even hours [26]. Another class of methods is the polarization-based technique proposed by Schechner et al. [26]. The major disadvantage of this method is camera setting which captures two strictly aligned polarized images only [2]. Another disadvantage is that it requires dedicated hardware for rotating the polarizer. The relevant methods in [21, 26–28] are not able to adapt themselves to practical scenarios since only one degraded image is available as an input; thus, more flexible approaches are preferable [26]. As a summary, the main disadvantage of these multiple image restoration methods is that several images with identical scene and dissimilar weather environments are required.

Single image restorations are a difficult task [23]. Nowadays, only one degraded image is available on which various algorithms can be applied [33]. In [9], an independent-component analysis algorithm was suggested. This method is related to local statistic and requires color information and variance. It achieves good results when the image is affected by thin fog but has trouble with dense fog where color is light-sensitive and the variance is not reliable to estimate the transmission map. The method in [9] is not suitable for grayscale images and requires deep knowledge of color. In another work [16], the restored image looks over saturated and unnatural looking. A different approach proposed in [11] called the deep photo system heavily relies on 3D model where no dehazing was performed if no model on the scene is available [1, 7, 45].

A more popular method that has been explored in recent years is using the dark channel prior (DCP) [19], which is one of the most simple, elegant and effective in single image defogging. Yong et al. [42] suggested the enhancement of Contrast Limited Adaptive Histogram Equalization (CLAHE) algorithm on the basis of archive monitoring and low illumination. Yadav et al. [40] argued how a digitally filtered image can be enhanced using CLAHE algorithm in order to improve its contrast. Other works on image handling can be seen in [22, 29, 30, 35–38].To sum up, some drawbacks of the single image restoration methods are shown as follows:

- Prominence of the reinstated image is very low.
- There are some Halo artifacts on the subsequent images.
- Some of these mentioned methods are unacceptable when a scene object is akin to air light like vehicle head lights, snow-white ground, etc.
- Correct prediction of transmission map is not estimated.
- Estimation of air light is not measured accurately.
- Improvement of the contrast of an image is difficult.
- More computational time.

It has been realized that CLAHE achieves good results compared to the other algorithms. In this article, we aim to enhance this algorithm by proposed a new method that combines Guided Filter and CLAHE for visibility improvement in fog removal. Our main contributions in this research are as follows:

- The proposed work uses Guided Filter for improvement of transmission map obtained from Median dark channel prior (MDCP), which is an improvement of the DCP with the new median operation. It has few data driven parameters and constants.
- The proposed method uses Contrast-Limited Adaptive Histogram Equalization (CLAHE) for visibility improvement of fog removal. In spite of the fact that there are different strategies for enhancing the view by expelling mist; however the greater part of them obliterates the shape and appearance of foggy images prompting a misdiagnosis. Thus, in this work CLAHE is utilized for identification of mist. The difference, particularly in homogeneous zones, can be constrained to abstain from intensifying any commotion that may be available in the image. It replaces each pixel in a given image by histogram of the surrendered areas to estimate pixels. Moreover, the CLAHE calculation is a broadly utilized system which brings differentiation improvement of images. Each tile's complexity is upgraded so that the histogram of the yield locale roughly coordinates that indicated by the 'Dispersion' parameter. CLAHE works on a little locale, called tile, as opposed to the whole image. It causes no harm on symptomatic outcomes. Alternate strategies utilized for the most part are: wavelet change, un-sharp concealing, and morphological administrator.
- The proposed method will be validated on the datasets in various types of climatic images against the relevant works namely Kopf et al.; Fattal's; Tan et al.; He et according to the evaluation metrics such as VM, PNSR and AMBE. The dataset contains more than 100 images of outside scenes and for each scene there are 5 unmistakable climate conditions are rehashed.
- The proposed method preserves small details while remaining robust against density of fog, and recovers scene contrast simultaneously. It is simple but effective in removing fog from a single degraded image. The proposed method operates at a high speed than existing ones and can minimize the halo artifact.
- To the best of our knowledge, none of the existing methods work well in three major factors (Contrast, Halo effect and transmission map) of fog removal simultaneously. Thus, we believe that the proposed method will put some extra value in this research field.

This article is organized into eight sections. Section 2 showsthe related works for fog removal. Section 3 shows the basic theory of atmospheric dichromatic model to describe the formation of fog. In Sections 4 and 5, we illustrate the proposed approach and its instantiation respectively. Experimental environment and performance evaluations of the proposed method are discussed in Sections 6 and 7 respectively. Finally, Section 8 concludes the research article and delineates further studies.

2 Related work

In this section, we discuss some previous approaches about fog removal techniques and their pros and cons (See Table 1).

3 Background

In computer vision, the atmospheric dichromatic model [21] is used in description of formation of foggy images as indicated in Fig. 1:

$$\hat{X}(a, b) = X(a, b)t(a, b) + a_{ir}(1−t(a, b)). \tag{1}$$

RGB color of the fog image $\hat{X}$ at pixel position (a. b) is expressed in Eq. 2:

$$\hat{X}(a, b) = \left[\hat{X}(a, b, r), \hat{X}(a, b, g), \hat{X}(a, b, b1) \right]^T. \tag{2}$$

RGB color image without fog at pixel position (a, b) is shown in Eq. 3:

$$X(a, b) = \left[X(a, b, r), X(a, b, g), X(a, b, b1) \right]^T. \tag{3}$$

In Eq. 1, the first term $X(a, b)$ $t(a, b)$ is called 'direct distortion' which produces a multiplicative distortion of scene radiance and reduces the contrast. The later term $a_{ir}(1 − t(a, b))$ is called the 'local atmospheric light distortion' which produces additive effects and adds the whiteness in a scene. Intuitively, an image received by observer is the combination of the attenuated version of underlying scene radiance with an additive atmospheric light [23]. The atmosphere is assumed to be homogenous [18]. This has two simplifying consequences: the atmospheric light is constant throughout the image (which means that it has to be estimated only once), and the transmission $t(a, b)$ follows the Beer-Lambert law in Eq.4:

$$t(a, b) = e^{−\beta d(a,b)}. \tag{4}$$

Here, β is the extinction coefficient and $d(a, b)$ represents the distance from the observer to the scene at pixel (a, b). When we assume the atmosphere is homogenous, it restricts β to be constant. The medium transmission coefficient has a scalar value within $0 \leq t(a, b) \leq 1$ for each pixel which attenuates the target color. Putting value of $t(a, b)$ in Eq. 1, we gain Eq. 5:

$$\hat{X}(a, b) = X(a, b)e^{−\beta d(a,b)} + a_{ir}\left(1−e^{−\beta d(a,b)}\right). \tag{5}$$

The main aim of fog removal is finding $X(a, b)$ which also requires information regarding of distance (d) between the scene and camera, extinction coefficient (β) and air light (a_{ir}). Eq. 5 indicates that the distance attenuates exponentially [13]. The depth up to an unknown distance can be recovered by recovering the transmission.

The ultimate goal of 'single image fog removal' is to recover a true image $X(a, b)$ from the observed fog-image $\hat{X}(a, b)$ which requires knowledge of three unknown parameters, β, d and a_{ir}. He et al. [11] introduced a successful algorithm of dark channel prior (DCP). Low value of

Table 1 A brief review of the related works

Method	Description	Pros	Cons
Polarization filter [26]	Air light is incompletely polarized. In this method, the input image is mixture of two unidentified mechanisms. The first one is the sight without the fog and another one is air light	Fog is detached by the polarization filter. No halo effect	Numerous images with similar scene and changed weather environments are compulsory
Dark channel prior (DCP) [11]	Some particular pixels consume small strength in any of the color channel	Single image is mandatory for haze elimination. Transmission map is evaluated correctly	Air light approximation hypothesis is required that only 0.1% positive pixels are reserved. It creates some halo effects on the resulting images
Improved dark channel prior (IDCP) [27]	Soft-matting is applied with the help of bilateral filter which smoothen the slight textures of image	Accurate estimated air light and less computation time	It creates halo effects in specific regions of the image. Transmission map is not projected correctly
IDCP using guided filter [12]	Image dehazing is completed by merging dark channel prior (DCP) and guided filter. Guided filter is an operator of preserve the edge and smoothen the image	Halo effects are detached proficiently. For the decent result, advanced transmission is applied by guided filter	It cannot be competent to develop the contrast of the image
DCP with histogram specification [41]	Recover the contrast of a recuperated image. Histogram of fog removal image has an affinity of left-shifting. Some sharpen area arises in the high concentrating region	Haze is detached from the huge contextual region and dump region of images. It enhances the contrast of fog free image	Size of the image and computation time are increased tremendously
Anisotropic diffusion method [6]	Post processing is used for the contrast enhancement which is appropriate for hazy images. The color model decreases the computation time	Estimation of air light is completed precisely. Contrast is boosted in the resulting image	Transmission map is not appraised correctly. Prominence of the reestablished image is poor
Parametric model, [24]	Hypothesis testing based on Long range transportation (LRT) detector	Compare LRT design by using the proposed one	The proposed method is hypotheticalimages re-sampled from mixed compressed and uncompressed images due to which uniformity is not maintained. It lacks of accurate model
Steganography, [39]	Steganalys is analysis was done using steganography tools	Calibration is done with features decreasing the influence of image content. It is helpful to detect stego messages hidden by Least significant bit (LSB) matching	Experimental results calculate non-adjacent pixels. Dependencies between the random pixel pairs were considered due to which the

Table 1 (continued)

| Method	Description	Pros	Cons
Image Retrieval Approach [4]	Standard texture databases and a color dataset show the benefits which can be drawn from the proposed retrieval approaches	Three different quantization schemes have been used. Quantization effect used in this work helps in efficient retrieval of fog	detection is influenced. Thus, it yields out non accurate results. Drops in the reduction of retrieval strategy are most likely to occur. It was carried out on 3 standard texture databases including a colored dataset. This mismatches the accurate results
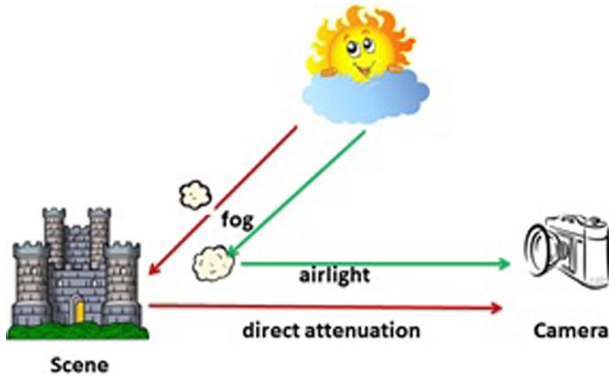
Fig. 1 The atmospheric dichromatic model

intensity is caused by lacking of color in a channel which may be due to shadows of buildings, trees and dark objects shown in Eq. 6.

$$\theta_D(a, b) = \min_{m,n \in \Omega(u,v)} \left(\min_{c \in (r,g,b)} \frac{X(a,b)^c}{a_{ir}(c)} \right). \qquad (6)$$

Thus, θ_D is used as a prior to estimate the transmission-map given by Eq. 7:

$$\widetilde{t_D}(a, b) = 1 - w\theta_D(a, b). \qquad (7)$$

The parameter $w(0 \leq w \leq 1)$ is introduced to prevent removing fog thoroughly and to keep the feeling of depth in a distant object as 0.95. The transmission obtained by Eq.7 is only a coarse estimation. If we try to recover $X(a, b)$ directly from Eq. 7, the result contains severe halo-artifact. Thus, it is necessary to refine the transmission. In order to remove these artifacts, transmission–map obtained by Eq. 7 is refined by using matting Laplacian in Eq.8:

$$E(t) = t^T Lt + \lambda \left(t - \widetilde{t_D} \right)^T \left(t - \widetilde{t_D} \right). \qquad (8)$$

The solution is found by solving for t_D from the following Eq. 9:

$$(L + \lambda U)t_D = \lambda \widetilde{t_D}. \qquad (9)$$

The (l,p) element of L is defined as in Eq. 10:

$$L(l, p) = \sum_{(k|l,p) \in w_k} \left(\delta_{l,p} - \frac{1}{|w_k|} \right) \left(1 + (X_i - \mu_k)^T \left(\textstyle\sum k + \frac{\varepsilon}{|w_k|} U_3 \right)^{-1} (X_j - \mu_k) \right), \quad (10)$$

where L is the $(MN \times MN)$ Matting Laplacian matrix for an image of size $(M \times N)$, $\delta_{l,p}$ is the Kronecker delta function, μ_k and $\sum k$ are the mean and covariance of the pixel in window (w_k) centered around k, $|w_k|$ is the number of pixels in each window, ε is a small regularization parameter (10^{-3} to 10^{-4}), U is an identity matrix with the same size as (L) and λ is a small value (10^{-3} to 10^{-4}) so that t_D is softly constrained by $\widetilde{t_D}$. Figure 2 indicates the result of recovered scene radiance using DCP followed by matting Laplacian. We can clearly see in Fig. 2d that the recovered de-foggy image contains some block artifact near the complicated edge structure.

In the proposed method, we conserved small details part of images when outstanding vigorous against concentration of fog, and recuperate scene contrast instantaneously. The new procedure is simple but actual in eliminating fog from a single tainted image. The proposed method controls at a high speed than existing approaches and can diminish the halo effect. Guided filter improves the transmission map acquired from Median dark channel prior
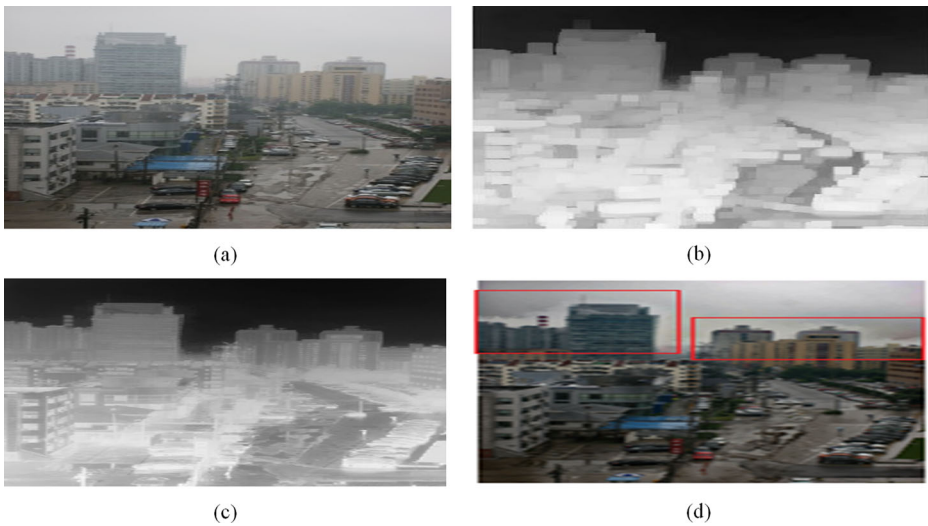
Fig. 2 Recovering the scene radiance using the transmission map refined by Matting Laplacian. **a** Original Fog Image, **b** Estimated Transmission Map from DCP, **c** Refined Transmission Map by Matting Laplacian, **d** Recovered Scene Radiance

(MDCP), which is an improvement of the Dark Channel Prior DCP by the use of median operation. All of the parameters used in our method are data driven.

4 The proposed work

4.1 Median dark-channel prior (MDCP)

We proposed a visibility restoration algorithm based on the utilization of median filtering operation. The proposed method is an improvement to the Dark Channel Prior [11] by replacing the second minimum operator in Eq. 6 with a median operator. The median operator performs a non-linear filtering operation which can effectively suppress impulsive noise components while preserving edge information in detailed areas and permitting dehazing [3, 8, 25] in smooth areas. The flow diagram of the algorithm is indicated in Fig. 3.

From a given foggy image, the atmospheric light, and transmission map are estimated. Once air light and transmission map are obtained, it is then refined by using the guided filter and scene radiance. To improve the overall contrast of an output image, CLAHE is performed as the post processing operation. The proposed median dark channel prior (MDCP) is given as Eq. 11:

$$\theta_M(a, b) = \operatorname*{med}_{m,n \in \Omega(a,b)} \left(\min_{c \in (r,g,b)} \frac{X(m, n)^c}{a_{ir}(c)} \right). \tag{11}$$

Here Ω represents a patch of size 15×15. Likewise, θ_M is then used to estimate the transmission-map given by Eq. 12:

$$\widetilde{t_M}(a, b) = 1 - w\theta_M(a, b). \tag{12}$$

The transmission map estimation using Eq. 12 can be used for further refinement. Despite several techniques soft matting [10], bilateral filter [14] and anisotropic diffusion [31] were

proposed to enhance the transmission map, they are computational intensive and may make the fog removal algorithm impracticable.

4.2 Transmission map refinement

The Matting Laplacian, which was used for refinement of transmission map in [11], produces visually satisfying results, but the computational cost is very high as it involves solving a large linear system. Therefore to speed up the defogging process, the transmission map obtained by Eq. 13 is refined by using the guided filter [12]. In the guided filter, kernel can be built by using a guidance image I_g and then applied to the target image $\widetilde{t_M}$ through a standard linear filtering process in the pixel domain. In general, the filtering process can be described by Eq. 14:

$$t_l = \sum_p W_{l,p}(I_g)\widetilde{t_J}, \tag{13}$$

$$W_{lp}(I_g) = \frac{1}{|w|^2}\sum_{k:(l,p)\in w_k}\left(1 + \frac{(I_l-\mu_k)(I-\mu_k)}{\sigma_k^2 + \varepsilon}\right), \tag{14}$$

where l and p are pixel indexes, t is the final result, W is the weight depending on the guidance image I_g, and $\widetilde{t_j}$ is the input image. For a color image, derivation of the guided filter relies on a linear assumption between the guidance image I_g and the refined transmission map t in Eq. 15.

$$t_l = a_k^T I_g + b_k, \forall_l \in w_k, \tag{15}$$

where t_l are the filter output, (a_k, b_k) are some linear coefficient's assumed to be constant in a window (w_k). Windows size is typically defined by their radius (r), which is the pixel distance from the center pixel to the outer pixel. Since square window are used, the total window size is therefore $(2r + 1) \times (2r + 1)$. The guided filter seeks for coefficient (a_k, b_k) that minimizes the difference between the output and input, by using following cost function in Eq. 16:

$$E(a_k, b_k) = \sum_{l \in w_k}\left(\left(a_k I_g + b_k - \widetilde{t}\right) + \varepsilon a_k^2\right), \tag{16}$$

where ε is a regularization parameter to prevent a_k from being too large. The solution of Eq. 16 is found as in Eq. 17(a & b):

$$a_k = \left(\sum_k \varepsilon U\right)^{-1}\left(\frac{1}{|w|}\sum_{l \in w_k} I_g \widetilde{t_J} - \mu_k \overline{t_k}\right) \tag{17a}$$

$$b_k = \overline{t_k} - a_k^T \mu_k \tag{17b}$$

Here, μ_k and σ_k^2 are the mean and variance of I_g in a window w_k, and $|w|$ is the number of pixels in w_k. $\overline{t_k}$ is the mean of t in w_k. $\sum_k$ is the 3×3 covariance matrix of I_g in w_k and U is a 3×3 identity matrix. Since a pixel l belongs to many windows, the final output t_l is averaged over all possible windows. After computing all filter coefficients (a_k, b_k) in the image, the final output is:

$$t_l = \frac{1}{|w|}\sum_{k:(l)\in w_k}\left(a_k^T Ig + b_k\right) \tag{18}$$

Thus, the guided filter simply measures the normalized correlation between two pixels. Spatial distance is taken into account by the fact that when two pixels l and p close together, they share more windows compared to when they are far apart.
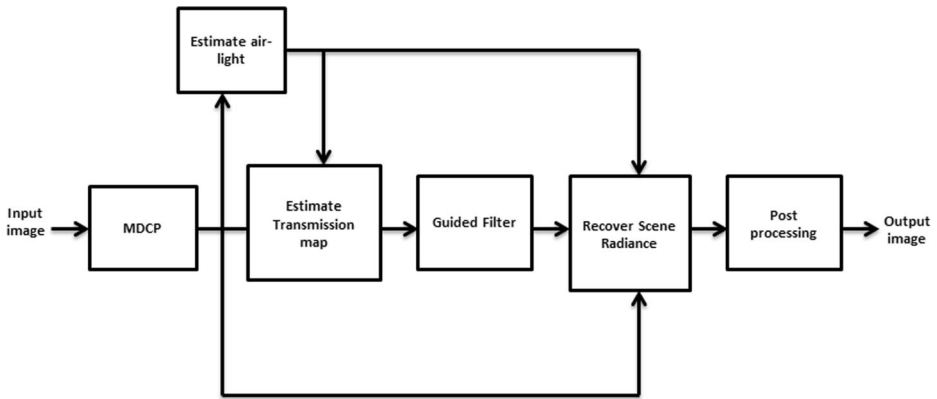
Fig. 3 Block Diagram of fog removal method

4.3 Behavior of guided filter

The input images are filtered by edge preserving smoothing filter, fast, accurate, non-iterative guided filter. The main benefit of this guided filter is that it has good behavior near edges and does not suffer from the problem of gradient-reversal artifact. Guided filter take advantages of reducing the problem of solving a large linear system of equations to a simple filtering process. It is demonstrated below.

Algorithm: Guided Filter

Input: Transmission map ($\tilde{t}$) , Guidance Image (I_g) , Regularization parameter (ε).

Output: Filtered transmission map t.

Step 1: Compute:

$$mean_{I_g} = f_{mean}(I_g),$$

$$mean_{\tilde{t}} = f_{mean}(\tilde{t}),$$

$$corr_{I_g} = f_{mean}(I_g.* I_g),$$

$$corr_{I_g\tilde{t}} = f_{mean}(I_g.* \tilde{t}).$$

Step 2: Calculate:

$$var_{I_g} = corr_{I_g} - mean_{I_g}.* mean_{I_g},$$

$$cov_{I_g\tilde{t}} = corr_{I_g.\tilde{t}} - mean_{I_g}.* mean_{\tilde{t}}.$$

Step 3: Compute:

$$a = cov_{I_g\tilde{t}}./var_{I_g} + \varepsilon,$$

$$b = mean_{\tilde{t}} - a.* mean_{I_g}.$$

Step 4: Compute the mean values:

$$mean_a = f_{mean}(a),$$

$$mean_b = f_{mean}(b).$$

Step 5: Finally calculate the transmission map:

$$t = f_{mean}(a).* I_g + f_{mean}(b).$$

4.4 Recovering the scene radiance

The map (t), and air light (a_{ir}) are known. The scene radiance can be estimated by using Eq. 19:

$$X(a, b) = \frac{\hat{X}(a, b) - a_{ir}}{\max(t, t_o)} + a_{ir} \qquad (19)$$

Using Eq. 19, t_o is typically bounded to a low number such as 0.1 to avoid instability. Figure 4 shows the result of a recovered scene radiance using the guided filter.

4.5 Post-Processing using CLAHE

It is found that image after removal of fog loses some contrasts and appears dim. This can improve the visibility. The most common method for visibility enhancement is the histogram equalization and histogram stretching. Histogram equalization is the most well-known methodby using the gray-scale transformation. However, its major disadvantage is that it over-enhances the image and shifts mean brightness and consequently creates an unnatural look. While in histogram stretching, we have to be careful of clipping; otherwise it eliminates visual information in bright and in dark region. Therefore, instead of using the histogram equalization and histogram stretching which affect the whole image, we use the CLAHE algorithm as indicated in Fig. 5a and b.

CLAHE is a visibility enhancement algorithm which can provide optimal equalization and overcome the problem of standard histogram equalization. As proposed in [34], CLAHE divides an images into small contextual region [8×8], and applies the histogram equalization to each region for contrast-enhancement. It also combines neighboring blocks into an image bilinear interpolation to eliminate artificially induced boundaries. There are two parameters in CLAHE to control image quality namely block-size and clip-limit. Block-size specifies the size of contextual-region, and clip-limit is a scalar parameter in range [0,1] specifying the contrast enhancement limit and preventing over-saturation. The CLAHE method can be derived from following steps in Eq. 20:

$$N_{avg} = \frac{N_x \times N_y}{N_{Gray}}. \qquad (20)$$

Based on Eq. 20, the N_{CL} can be calculated by Eq. 21:

$$N_{CL} = N_{clip} \times N_{avg}, \qquad (21)$$

Fig. 4 Behavior of guided filter after filtering, the edges of the guide image is transferred to the filtering image: **a** Noisy Image, **b** Guidance image, **c** Image after guided filtering
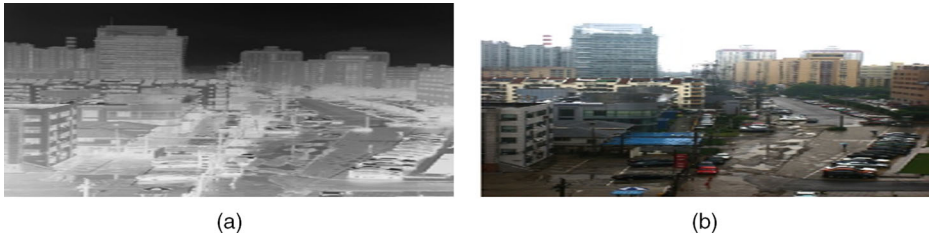
(a)

(c)

(b)

(a)   (b)
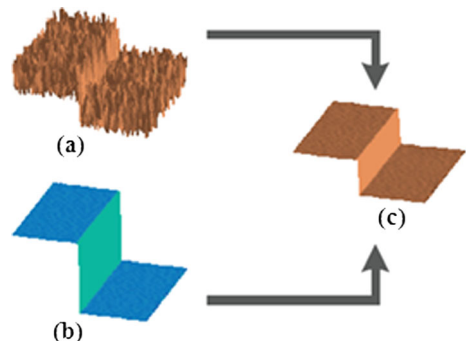
Fig. 5 Recovering scene radiance using the MDCP and Guided Filter: **a** Enhanced Transmission Map by Guided Filter, **b** Restored Scene Radiance

where,

N_{avg}	Average Number of Pixels.
N_x	Number of pixels in X-axis.
N_y	Y-axis.
N_{Gray}	Number of gray levels.
N_{CL}	Actual Clip-Limit.
N_{clip}	Maximum multiple of average pixels in each gray level.

The original and clipped histograms are indicated in Fig. 6a. We can observe in Fig. 6b that if pixels are greater than N_{clip}then they result in clipping of the pixels. $N_{\sum clip}$ Indicates the total numbers of clipped pixels in each gray level given in Eq. 22:

$$N_{acp} = \frac{N_{\sum clip}}{N_{gray}}. \tag{22}$$

The contextual region can be calculated by using the following rules:

- *Rule 1:* If $N_x(i) > N_{CL}$, $N_x(i) = N_{CL}$
- *Rule 2:* Elseif $N_x(i) + N_{acp} \geq N_{CL}$, $N_x(i) = N_{CL}$
- *Rule 3:* Else $N_x(i) = N_x(i) + N_{ap}$

The step of distributed pixels can be calculated by using the Eq. 23:

$$S = \frac{N_{Gray}}{N_{RP}}, \tag{23}$$
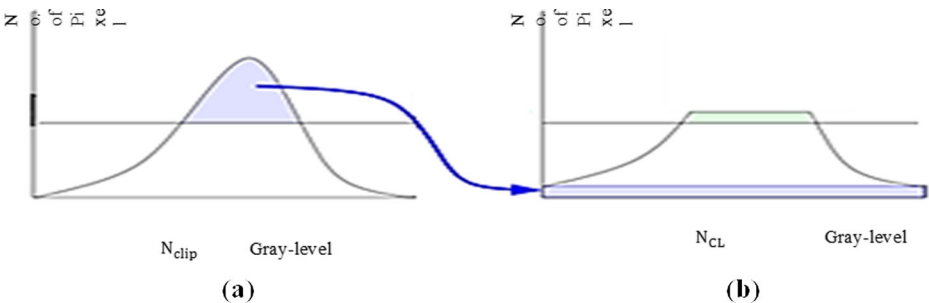
where N_{RP} denotes the remaining number of clipped pixel.

Fig. 6 Representation of the original and clipped histogram (CLAHE): **a** Original histogram **b** Clipped histogram

4.6 Description of the proposed algorithm

The algorithm is shown in Table 2 where I is the input image and I_F is the output. The time complexity of the guided filter algorithm (Steps 3 and 4) is $O(n)$ where n is number of the pixels in the image. The time complexity of other procedures like MDCP, transmission map refinement, recovering scene radiance and CLAHE is O(1). Therefore, the total time complexity is $(O(n) + O(1)) = O(n)$.

5 Instantiation

In any case, using a clock rate comparable to pixel landing rate, the mean number of required mapping RAMs is 32. For this circumstance, when all operations are driven at the pixel passage rate, there is a prerequisite for another extra eight mapping RAM's to fill in as a pad for authentic pipe covering of all operations. The time laps between utilization of the fundamental regional mapping sequentially and the last common mapping in a comparative segment, for 512×512 pictures, is, at most, proportional to the arrival time of $7 \times 64 = 448$ pixels. Under best conditions, using a higher clock rate, the base required number of mapping RAM's is 24. The accompanying and last operation is to framework of the image, as shown by the most ideal blend of the regional mappings. For the underlying 32 sections of an image, only eight commonplace mappings are required. The final pixel mapping is planned based on the assumption that regional mappings are available for the pixel under process. Realization of this engine depends on the way that six products are

Table 2 The proposed method

Input: I is the input image
Output: I_F (Fog / haze removed image)
Algorithm:
1. Apply the Median Dark Channel Prior (MDCP) to the image I and calculate θ_M to estimate the transmission map t_M.
2. The output of MDCP t_M is converted to refined transmission map t_l using transmission map refinement.
3. Guided filtering algorithm is applied to the transmission map. The inputs of this algorithm are transmission map (tl), guidance image (I_g), regularization parameter (ε). The output is filtered transmission map t.
4. Recover the scene radiance using known parameters i.e. the filtered transmission map (t), and air light (a_{ir}).
5. Process the final image in the Post-Processing step using CLAHE for visibility enhancement.
6. Finally we get the final output as I_F (Fog removed image).

calculated. It is possible to simplify hardware realization as follows. Let η and μ be defined as

$$\eta = \frac{X}{X + Y},$$
$$\mu = \frac{S}{R + S}.$$

This mapping can be solved by using the following given equation:

$$P_{new} = \mu \big[\eta\, f_{i-1, j-1}(P_{old}) + (1-\eta)\, f_{i, j-1}(P_{old}) \big] + (1-\mu) \big[\eta\, f_{i-1, j}(P_{old}) + (1-\eta)\, f_{i, j}(P_{old}) \big].$$

Since the scales in the multipliers, for square districts with size of forces of two, are dyadic numbers, the multipliers may have more productive equipment usage. The quantity of time-keepers expected to finish each mapping operation relies upon how the multipliers are executed. In the event that the multipliers are likewise legitimately pipelined, with an inertness of at most 30 pixels, for every pixel entry, one-pixel mapping is finished. On account of 512 square images, the locales are of size 64 by 64 and the scaling factors are numbers separated by 64.

6 Experimental setup

This section presents an assessment of the proposed method by using MATLAB 7.0.4, 64-bit Intel Core i3–2600 processor with memory of 2GB. To compare the performance of our method, benchmark images such as foggy images namely Mountain '01', Tower '02', 'Sweden' are derived from well-known sources in Google database. The Haze RD dataset contains 15 actual outdoor scenes, and for each scene there are 5 different climate conditions are replicated. Besides, we also collected more than 50 extra images with different outdoor scene and added to the Haze RD dataset for the experiment. Thus, in this experiment we use more than 100 images for verifying the proposed method. The objective of evaluation is to check how well the images are restored by the algorithm. In order to do so, image quality metrics are necessary to assess the quality of images. Performance of the algorithms are measured in terms of Visibility Metric (VM), Absolute Mean Brightness Error (AMBE), Peak Signal to Noise Ratio (PSNR), and Run Time (t_{comp}).

6.1 Visibility metric (VM)

The visually enhancement performance is defined by visibility metric. Visibility is a measure of image quality and used to tell how well an observer can view a texture and color of image.

Table 3 Run time (seconds) comparison of the proposed method with the other methods

Method	t_{run}(mean ± SD)
Kim et al. [15]	$21.16 \pm 4.2 \times 10^{-3}$
Fattal [9]	$19.36 \pm 4.2 \times 10^{-3}$
Kopf et al. [17]	$17.48 \pm 7.2 \times 10^{-3}$
He et al. [11]	$15.42 \pm 4.2 \times 10^{-3}$
Ren et al. [25]	$16.24 \pm 5.1 \times 10^{-3}$
Berman and Avidan [3]	$15.34 \pm 5.2 \times 10^{-3}$
Fan et al. [8]	$13.38 \pm 6.2 \times 10^{-3}$
Proposed Method	$5.12 \pm 7.2 \times 10^{-3}$

(a)   (b)

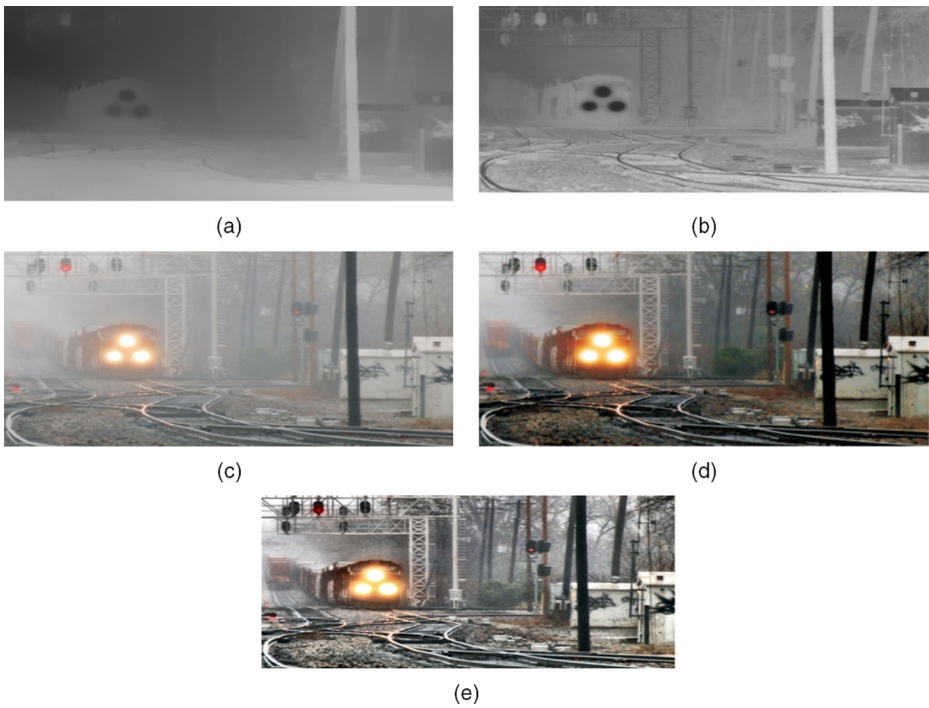(c)   (d)

(e)

Fig. 7 Intermediate steps of proposed method: **a** Original fog image 'train' **b** Estimated Transmission map using MDCP, **c** Enhanced transmission map using Guided filter **d** Restored image **e** Final fog free image followed by post- processing

Visibility metric gives an objective measure of detail enhancement. The enhancement in contrast and edge sharpness is useful for measuring the enhancement. The visibility metric is calculated in Eqs. 24, 25, 26, 27 and 28.

$$n(l, p) = r(l, p) - e(l, p), \tag{24}$$

$$\mu_r = \frac{1}{M \times N} \sum_{i=0}^{M-1} \sum_{i=0}^{N-1} r(l.p), \tag{25}$$

$$\mu_n = \frac{1}{M \times N} \sum_{i=0}^{M-1} \sum_{j=0}^{N-1} n(l, p), \tag{26}$$

$$\sigma_n^2 = \frac{1}{(M \times N) - 1} \sum_{i=0}^{M-1} \sum_{i=0}^{N-1} (n(l, p) - \mu_n)^2, \tag{27}$$

$$VM = CNR(r, e) = \frac{\mu_r - \mu_n}{\sigma_n}. \tag{28}$$

r (l, p) and e(l, p) denote the image taken as reference and improved images (M × N), n(l,p) visibility of the image, μ_n, μ_r and σ_n^2, are mean and variance. The effectiveness is described by high value of visibility metric.
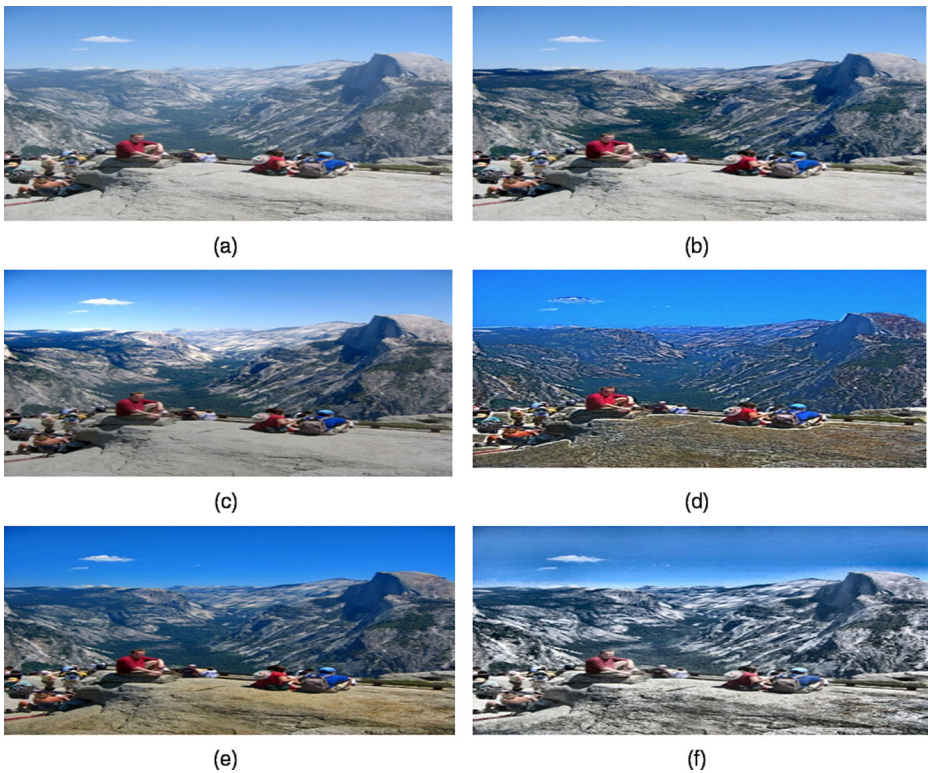
(a)

(b)

(c)

(d)

(e)

(f)

Fig. 8 Visual comparison of defogging result with recent state-of-the-art methods: **a** Original foggy image 'mountain 01' recovered by the algorithm; **b** Kopf et al.; **c** Fattal's; **d** Tan et al.; **e** He et al.; **f** The proposed algorithm

6.2 Absolute mean brightness error (AMBE)

A qualitative measure of visibility enhancement is checked in terms of AMBE. To examine how the appearance of image has changed after removal of fog, the deviation of the reference image is computed in Eq. 29.

$$\text{AMBE} = |\mu_r - \mu_n|. \tag{29}$$

For better similarity between two images, the AMBE must be as small as possible.

6.3 Peak signal to noise ratio (PSNR)

There are many version of SNR, but the PSNR are simpler and widely used for fidelity measurement. PSNR, calculated in decibels units, measures the ratio of the peak signal (Eq. 30) and the Mean-Square-Error between two images. It is defined in Eq. 31:

$$\text{MSE} = \frac{1}{M \times N} \sum_{i=0}^{M-1} \sum_{i=0}^{N-1} (r(l, p) - e(l, p))^2, \tag{30}$$

$$\text{PSNR} = 10 \log_{10} \left(\frac{(L-1)^2}{\text{MSE}} \right), \tag{31}$$

Fig. 9 Visual comparison of defogging result with recent state-of-the-art methods: **a** Original hazy image 'tower 02' recovered by the algorithm; **b** Kopf et al.; **c** Fattal's; **d** Tan et al.; (e) He et al.; **f** The proposed algorithm

where r(l,p) denotes the original foggy image and e(l,p) denotes the enhanced fog-free image. (M × N) represents the size of image and L is dynamic range of pixel values (256 for 8-bit grayscale image).

6.4 Run time(t_{run})

Run time (t_{run}) is the period during which the computer program is executing to remove fog from image. Therefore, the efficiency of an image depends on how fast the algorithm is. For the fog removal, t_{run} is related to the size of image. For fast execution, t_{run} must be low. (Table 3).

7 Results and discussions

Firstly, intermediate steps of proposed method are illustrated in Fig. 7.

To check the effectiveness of the proposed method, we carry out simulation on various foggy images: Mountain'01′, Tower '02', 'Sweden' in Figs. 8, 9 and 10.

The Visibility Metric in comparison with other methods is shown in Table 4 in which the 2nd column represents the actual visibility of fog images whereas the restored visibility are depicted in last column of this table. We observe that actual visibility of the fog image-
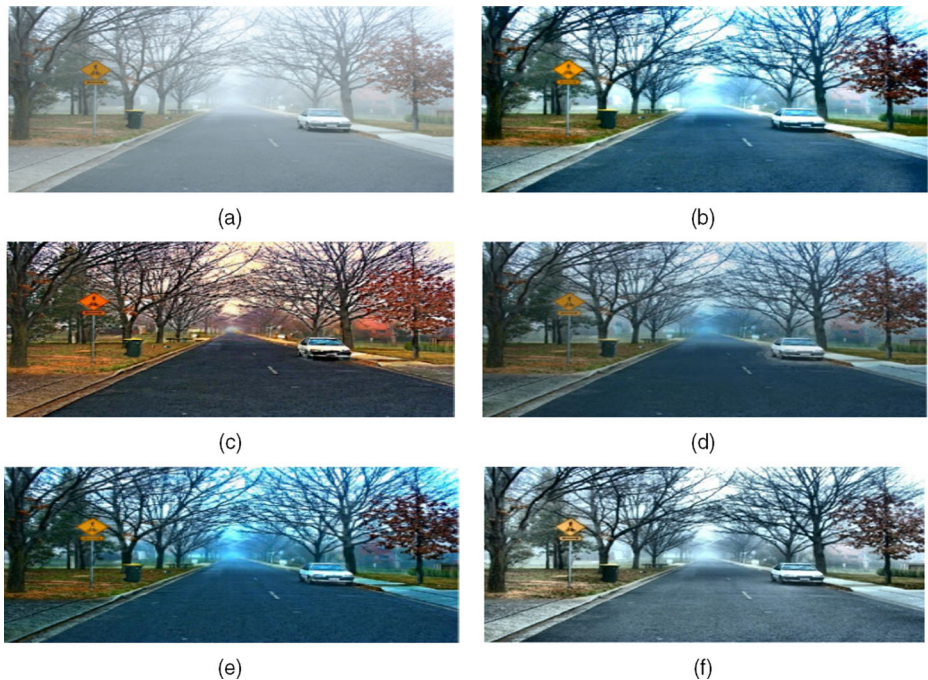
Fig. 10 Visual comparison of defogging result with recent state-of-the-art methods: **a** Original hazy image 'Sweden', recovered by the algorithm; **b** Kopf et al.; **c** Fattal's; **d** Tan et al.; **e** He et al.; **f** The proposed algorithm

Mountain '01' is 70.59 which is increased to 115.62 after fog removal. Similarly, in Tables 5 and 6, we compare the PSNR and AMBE with the other state-of-art methods. The effectiveness of the proposed method is described by high value of VM and low value of AMBE, ηand t_{run}.

Likewise, from Table 4, the visibility metric produced by the proposed method yields out 40% more enhanced visibility than the others. The PSNR produced by the proposed method is 12.5% more than those of the existing works (Table 5). Especially for Mountain 01, the proposed method achieves 36% higher value of PSNR than that of He et al. However, AMBE comparison in Table 6 indicates that the proposed method works well with the ambience of the other but does not yield out effective results. The proposed method gives from 3% to 5% of PSNR more than Kopf et al., and Tan et al. for Tower '02'. The experimental result clearly indicates that the proposed method has the best result over all other approaches. Knowing the ground truth of any degraded images have been a difficult issues since long. However, we have adopted a common and well-known manually investigated image pixels into foreground and

Table 4 Visibility metric comparison produced by the proposed method and others

Image	VM	Kopf et al.	Fattal et al.	Tan et al.	He et al.	Ren et al.	Berman et al.	Fan et al.	Proposed Work
'Mountain 01'	70.59	80.14	78.18	76.62	87.95	88.96	87.98	89.58	115.62
'Tower 02'	65.92	99.61	99.26	97.48	103.41	104.52	105.12	104.84	150.63
'Sweden'	62.99	100.87	85.21	114.15	113.24	105.63	104.98	103.25	115.98

Table 5 PSNR comparison produced by the proposed method and others

Image	Kopf et al.	Fattal et al.	Tan et al.	He et al.	Ren et al.	Berman et al.	Fan et al.	Proposed Work
'Mountain 01'	34.83	45.74	30.07	32.16	33.54	34.63	36.84	48.40
'Tower 02'	31.47	36.82	28.62	33.87	34.85	37.85	34.14	42.83
'Sweden'	22.67	22.71	22.50	24.60	25.36	24.52	24.62	28.74

background classes. These include presence of degradation effects such as lack of contrast, interfering patterns and color fading. We have identified these images as degraded in the following way:

a) The difficulty in taking a decision that which pixel should be considered as text or background as the pixels are mislabeled is such images. Hence, they are mentioned in our work as haze images (Misty, Foggy, Cloudy Images).
b) The confusion between text and background rises which makes the separation task quite difficult (gray-scale intensity). We found these RGB (Red, Green Blue) images with redundant luminance information. Thus, these segments appear as if they are fog. This happens in most of the historical and old images.

Now, we compare all algorithms on the HazeRD dataset [44] with respect to the Average VM (Avg_VM), Average PSNR (Avg_PSNR) and Average AMBE (Avg_AMBE). In Table 7, it is clear that the proposed method produces the highest average VM and PSNR values and lower AMBE values. It has been shown that the proposed method gives the best result over all.

Figures 11 and 12 demonstrate defogging of the proposed method and the others. An illustration of refining the transmission map using the guided filter with various window sizes is indicated in Fig. 13a and b. Herein, we adapt a simple strategy to adjust r^{dark} according to the area of image. When the number of pixels in the image is less than (2×10^5), the radius is fixed as 15 preventing the patch size become too small. When the number of pixels is more than (2×10^5), the radius is fixed as 30, preventing the patch size from growing too large. For the guided filter, the regularization parameter ε fix to be 10^{-2}. The parameter t_o is set to be 0.1, but its value needs to be increased when an image contains sky regions. The parameter $\lambda = 10{-}4$ is chosen corresponding to the best PSNR. The value of parameter wis depended on applications but we fix it to 0.95 for all result reported in this paper.

An important parameter for computing the dark channel is patch size. We denote its radius as r^{dark}. Since the computational cost in soft matting is quite high, we cannot use it for refinement of large images. In [12], the patch size is fixed as 15×15 which is relatively small. However, the complexity of the proposed method is quite low, and it is capable of processing

Table 6 AMBE comparison of the proposed method and others

Image	Kopf et al.	Fattal et al.	Tan et al.	He et al.	Ren et al.	Berman et al.	Fan et al.	Proposed Work
Mountain'01'	22.61	17.86	47.97	48.27	38.52	34.21	35.27	10.92
Tower '02'	16.54	34.46	47.80	34.88	31.24	30.14	31.42	5.51
Sweden	45.00	76.38	75.86	71.06	68.54	67.52	54.21	43.58

Table 7 Comparison on the Haze RD dataset in terms of the basic comparative factors

Method	Avg_VM	Avg_PSNR	Avg_AMBE
Tan et al. (2011)	102.89	25.98	59.98
Fattal [9]	88.56	38.09	62.28
Kopf et al. [17]	91.25	30.68	43.89
He et al. [11]	108.98	31.87	55.76
Ren et al. [25]	108.92	21.27	46.85
Berman and Avidan [3]	109.81	24.47	47.89
Fan et al. [8]	112.28	29.57	41.29
Proposed Method	131.85	40.78	41.65

the large image with short running time. Thus, it is not appropriate to use fixed patch size. From the local linear model in Section 4, large radius r implies that filtering output is linear to guidance images in order to reduce the halo artifact in recovered image. But if r is too large, the transmission map will capture too much detail from the guidance; making the recovered image over saturated. Failure of transmission refinement using the guided filter is indicated in Fig. 14a and b.

In those images, the uppermost right corner is destroyed because of using DCP. The dark channel prior (DCP) is statistically based; thus it is likely that particular spots in the image do not follow this prior. Indeed, this method fails when some objects in a particular image is inherently gray or white. It assumes that a part of the images is a part of the fog. That is why the white patches are appeared in the image. Our method may misjudge the fatness of the haze (underestimate the transmission). Thus, the color saturation is occurred in the recovered image.

Fig. 11 Defogging of the proposed method vs. He et al. method **a** Input image, **b** He's result, **c** Proposed method's **d** Input image, **e** He's result, **f** Proposed method's
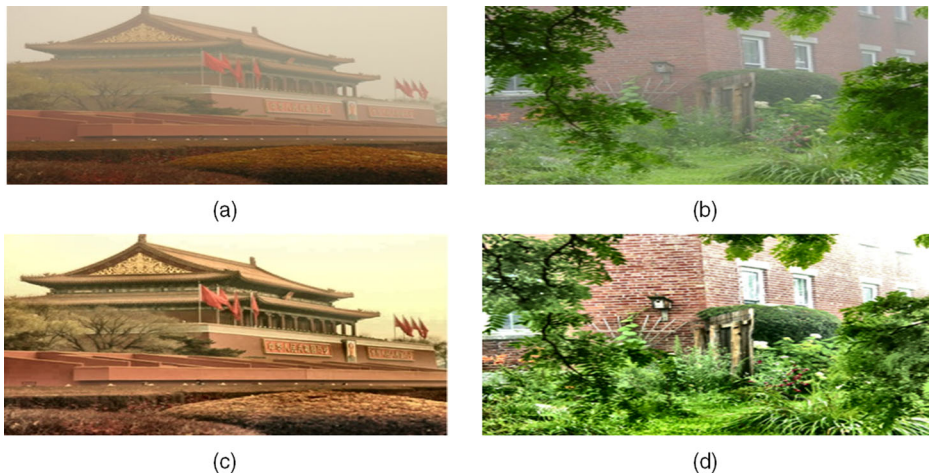
(a)　　　　　　　　　　　　　　　　　　(b)

(c)　　　　　　　　　　　　　　　　　　(d)

Fig. 12 Defogging for heavy fog images by the proposed method: **a** Foggy 'Monastery' image, **b** Foggy 'Hostel' image, **c** Restored 'Monastery' image, **d** Restored 'Hostel' image

In the future, we will try to use Edge Aware Filtering to overcome this limitation. Edge-aware filtering become inherent, e.g. through answering a linear arrangement. The weighted least squares (WLS) filter uses the matrix operations according to gradient of the image. There are two cases in Edge-aware filtering such as Flat patches and Edge or high variance. When a pixel is in the center of a flat patch region, its value is converted into the average of adjacent pixels. If it is in the center of an edge or high variance region, its value will be constant. Because edge-aware filter is time consuming, we can try minimizing the time complexity of this filter by using fast and high quality explicit filter.

8 Conclusion

Through the survey on state-of-the-arts on fog removal, it is a fact that they ignored every phase or circumstances. The existing techniques neglect utilization of the dark channels prior to reduce noises and uneven illuminate problems. To overcome the previous circumstance, we proposed in this paper an integrated algorithm to improve the visibility of fog degraded images. It is a combination of Guided filter and CLAHE, where the Guided filter is an edge-preserving filter which is used for quickly refinement of transmission map and CLAHE
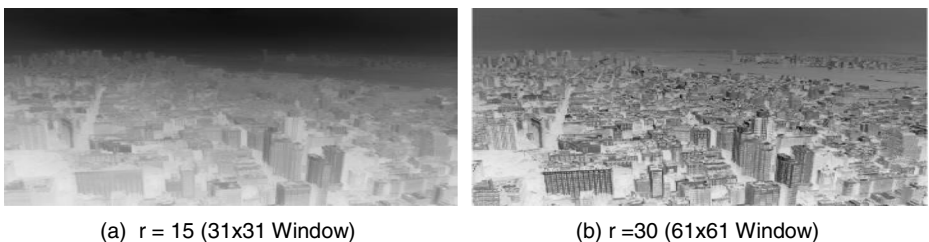

(a) r = 15 (31x31 Window)　　　　　　　(b) r =30 (61x61 Window)

Fig. 13 Refining the transmission map using guided filter with various window sizes ($\varepsilon = 10^{-2}$)

(a)   (b)

Fig. 14 Failure of suggested image: **a** Foggy input image and **b** Our result

is used to improve the local contrast of image by portioning the image into small boxes. The proposed methods has been empirically validated on benchmark images such as foggy images namely Mountain '01', Tower '02', 'Sweden', and the HazeRD datasets. Performance of the algorithms were measured in terms of Visibility Metric (VM), Absolute Mean Brightness Error (AMBE), Peak Signal to Noise Ratio (PSNR), and Run Time (t_{comp}).It was observed that in restored image, no oversaturated region exist due to which there is a negligible appearance of halo-artifact. The advantages of proposed method are multiple: It is simple in principle and hence easy to implement; it provides good result in most cases (homogenous fog), without introducing artifact and efficient for various type of fog images.

The proposed method outperforms the other existing methods by enhancing details in fog degraded images. However, guided image filtering is actually an approximation of soft matting; this method fails when the input image contains abrupt depth changes. Failure of transmission refinement using guided filter is aforementioned. To address the mention problem, we will try to use Edge Aware filtering with weighted least squares (WLS) filter. The idea is intuitively: when a pixel is in the center of a flat patch region, its value is converted into the average of adjacent pixels. If it is in the center of an edge or high variance region, its value will be constant. Because edge-aware filter is time consuming, we can try minimizing the time complexity of this filter by using fast and high quality explicit filter. All of these will be our future works in progress.

Compliance with ethical standards

Conflict of interest The authors declare that they have no conflict of interest.

References

1. Aizenberg I, Bregin T, Butakoff C, Karnaukhov V, Merzlyakov N, Milukova O (2002) Type of blur and blur parameters identification using neural network and its application to image restoration. Artificial Neural Networks:138–139
2. Ancuti C, Ancuti C, Hermans C, Bekaert P (2011) A fast semi-inverse approach to detect and remove the haze from a single image. Computer Vision–ACCV:501–514

3. Berman D, Avidan S (2016) Non-local image dehazing. In: CVPR, https://www.eng.tau.ac.il/~berman/NonLocalDehazing/index.html

4. Chaker A, Kaaniche M, Benazza-Benyahia A, Antonini M (2018) Efficient transform-based texture image retrieval techniques under quantization effects. Multimed Tools Appl 77(1):1–25

5. Cheng FC, Cheng CC, Lin PH, Huang SC (2015) A hierarchical airlight estimation method for image fog removal. Eng Appl Artif Intell 43:27–34

6. Dobler G, Cholis I, Weiner N (2011) The Fermi gamma-ray haze from dark matter annihilations and anisotropic diffusion. Astrophys J 741(1):25–34

7. Dong W, Zhang L, Shi G, Wu X (2011) Image deblurring and super-resolution by adaptive sparse domain selection and adaptive regularization. IEEE Trans Image Process 20(7):1838–1857

8. Fan X, Wang Y, Tang X et al (2017) Two-Layer Gaussian Process Regression with Example Selection for Image Dehazing. IEEE Transactions on Circuits & Systems for Video Technology 27(12):2505–2517

9. Fattal R (2014) Dehazing using color-lines. ACM Trans Graph 34(1):13–27

10. He K, Sun J (2015) Fast guided filter. arXiv preprint arXiv:1505.00996, 54, 147–158

11. He K, Sun J, Tang X (2011) Single image haze removal using dark channel prior. IEEE Trans Pattern Anal Mach Intell 33(12):2341–2353

12. He K, Sun J, Tang X (2013) Guided image filtering. IEEE Trans Pattern Anal Mach Intell 35(6):1397–1409

13. Huang SC, Chen BH, Wang WJ (2014) Visibility restoration of single hazy images captured in real-world weather conditions. IEEE Transactions on Circuits and Systems for Video Technology 24(10):1814–1824

14. Jiang J, Hou T, Qi M (2011) Improved algorithm on image haze removal using dark channel prior. Journal of circuits and systems 16(2):7–12

15. Kim JH, Sim JY, Kim CS (2011) Single image dehazing based on contrast enhancement. In: Proc. 2011 IEEE International Conference on Acoustics, Speech and Signal Processing (ICASSP), Prague, Czech Republic, pp 1273–1276

16. Kim JH, Jang WD, Sim JY, Kim CS (2013) Optimized contrast enhancement for real-time image and video dehazing. J Vis Commun Image Represent 24(3):410–425

17. Kopf J, Neubert B, Chen B, Cohen M, Cohen-Or D (2008) Deussen, O.,& Lischinski, D. Deep photo: Model-based photograph enhancement and viewing ACM 27(5):116–124

18. Kundur D, Hatzinakos D (1998) A novel blind deconvolution scheme for image restoration using recursive filtering. IEEE Trans Signal Process 46(2):375–390

19. Levin A, Lischinski D, Weiss Y (2008) A closed-form solution to natural image matting. IEEE Trans Pattern Anal Mach Intell 30(2):228–242

20. Levin A, Weiss Y, Durand F, Freeman WT (2011) Understanding blind deconvolution algorithms. IEEE Trans Pattern Anal Mach Intell 33(12):2354–2367

21. Narasimhan SG, Nayar SK (2003) Contrast restoration of weather degraded images. IEEE Trans Pattern Anal Mach Intell 25(6):713–724

22. Ngan TT, Tuan TM, Son LH, Minh NH, Dey N (2016) Decision Making Based on Fuzzy Aggregation Operators for Medical Diagnosis from Dental X-ray images. J Med Syst 40(12):1–7

23. Park D, Ko H (2012) Fog-degraded image restoration using characteristics of RGB channel in single monocular image. 2012 IEEE International Conference on Consumer Electronics, (pp. 139–140)

24. Qiao T, Zhu A, Retraint F (2018) Exposing image resampling forgery by using linear parametric model. Multimed Tools Appl 77(2):1501–1523

25. Ren W, Liu S, Zhang H, Pan X, Cao J, Yang MH (2016) Single image dehazing via multi-scale convolutional neural networks. In: ECCV, (pp.154–169)

26. Schechner YY, Narasimhan SG, Nayar SK (2001) Instant dehazing of images using polarization. Proceedings of the 2001 IEEE Computer Society Conference on Computer Vision and Pattern Recognition, 1, (pp. 124–134)

27. Shi L, Cui X, Yang L, Gai Z, Chu S, Shi J (2016) Image Haze Removal Using Dark Channel Prior and Inverse Image. MATEC Web of Conferences 75:30–38

28. Shi J, Malik J (2000) Normalized cuts and image segmentation. IEEE Trans Pattern Anal Mach Intell 22(8): 888–905

29. Son LH, Tuan TM (2016) A cooperative semi-supervised fuzzy clustering framework for dental X-ray image segmentation. Expert Syst Appl 46:380–393

30. Son LH, Tuan TM (2017) Dental segmentation from X-ray images using semi-supervised fuzzy clustering with spatial constraints. Eng Appl Artif Intell 59:186–195

31. Sun XM, Sun JX, Zhao LR, Cao Y (2014) Improved algorithm for single image haze removing using dark channel prior. Journal of Image and Graphics 19(3):381–385

32. Tai YW, Tan P, Brown MS (2011) Richardson-lucydeblurring for scenes under a projective motion path. IEEE Trans Pattern Anal Mach Intell 33(8):1603–1618

33. Tan RT (2008) Visibility in bad weather from a single image. IEEE Conference on Computer Vision and Pattern Recognition, (pp. 1–8)

34. Tang K, Yang J, Wang J (2014) Investigating haze-relevant features in a learning framework for image dehazing. Proceedings of the IEEE Conference on Computer Vision and Pattern Recognition, (pp. 2995–3000)

35. Tuan TM, Duc NT, Hai PV, Son LH (2017) Dental diagnosis from X-Ray images using fuzzy rule-based systems. International Journal of Fuzzy System Applications 6(1):1–16

36. Tuan TM, Ngan TT, Son LH (2016) A novel semi-supervised fuzzy clustering method based on interactive fuzzy satisficing for dental x-ray image segmentation. Appl Intell 45(2):402–428

37. Vo BN, Vo BT, Hoang H (2016) An Efficient Implementation of the Generalized Labeled Multi-Bernoulli Filter. IEEE Trans Signal Process 65(8):1975–1987

38. Wang G, Ren G, Jiang L, Quan T (2013) Single image dehazing algorithm based on sky region segmentation. Inf Technol J 12(6):1168–1175

39. Xia Z, Wang X, Sun X, Liu Q, Xiong N (2016) Steganalysis of lsb matching using differences between nonadjacent pixels. Multimed Tools Appl 75(4):1947–1962

40. Yadav G, Maheshwari S, Agarwal A (2014) Foggy image enhancement using contrast limited adaptive histogram equalization of digitally filtered image: Performance improvement. 2014 IEEE International Conference on Advances in Computing, Communications and Informatics, (pp. 2225–2231)

41. Yang S, Zhu Q, Wang J, Wu D, Xie Y (2013) An improved single image haze removal algorithm based on dark channel prior and histogram specification. In Proceedings of 3rd International Conf. On Multimedia Technology, Atlantis Press (pp. 279–292)

42. Yong W, Ting L, Yongsheng Q (2015) Image enhancement algorithm research based on the archives monitoring under low illumination. 2015 12th IEEE International Conference on Electronic Measurement & Instruments, 3, (pp. 1270–1274)

43. Yuan L, Sun J, Quan L, Shum HY (2007) Image deblurring with blurred/noisy image pairs. ACM Trans Graph 26(3):1–12

44. Zhang Y, Ding L, Sharma G (2017) HAZERD: an outdoor scene dataset and benchmark for single image dehazing, ICIP-2017, IEEE, (pp. 3205–3209)

45. Zhao S, Shmaliy YS, Liu F (2016) Fast Kalman-like optimal unbiased FIR filtering with applications. IEEE Trans Signal Process 64(9):2284–2297

Rajiv Kapoor received M.E. and Ph.D. degree in Electronics & Communication Engineering from Delhi College of Engineering, Delhi University. Dr. Kapoor presently working as Professor in Electronics & Communication Engineering Department, AIACT&R (Govt. of NCT of Delhi). He has authored over 90 research papers in various renowned international journal and conferences. His primary research interests are machine learning, computer vision, signal and image processing.

Rashmi Gupta received M.E. and Ph.D. degree in Electronics & Communication Engineering from Delhi College of Engineering, Delhi University. Dr. Gupta held the position of Sr. Engineer in Calcom group of companies from 1991 to 1999, position of Lecturer in Electronics & Communication Engineering Department at Hindu Institute of Technology and Senior Lecturer in Maharaja AgrasenIntitute of Technology, Delhi from 1999 to 2003. Dr. Gupta presently working as Associate Professor in Electronics & Communication Engineering Department, AIACT&R (Govt. of NCT of Delhi). She has authored over 40 research papers in various renowned international journal and conferences. Her primary research interests are machine learning, computer vision, signal and image processing.

Le Hoang Son obtained the PhD degree on Mathematics – Informatics at VNU University of Science, Vietnam National University (VNU) in 2013. He has been promoted to Associate Professor in Information Technology since 2017. Dr. Son worked as senior researcher and Vice Director at the Center for High Performance Computing, VNU University of Science, Vietnam National University during 2007–2018. From August 2018, he is Head of Department of Multimedia and Virtual Reality, VNU Information Technology Institute, VNU. He is also the Consultant of Vietnam Office of the Government from October 2018. His major fields include Artificial Intelligence, Data Mining, Soft Computing, Fuzzy Computing, Fuzzy Recommender Systems, and Geographic Information System. He is a member of International Association of Computer Science and Information Technology, Vietnam Society for Applications of Mathematics, and Key Laboratory of Geotechnical Engineering and Artificial Intelligence in University of Transport Technology (Vietnam). Dr. Son is an Associate Editor of Journal of Intelligent & Fuzzy Systems (SCIE), IEEE Access (SCIE), Neutrosophic Sets and Systems (ESCI), Vietnam Research and Development on Information and Communication Technology, VNU Journal of Science: Computer Science and Communication Engineering, Frontiers in Artificial Intelligence. He serves as Editorial Board of Applied Soft Computing (SCIE), PLOS ONE (SCIE), International Journal of Ambient Computing and Intelligence (ESCI), and Vietnam Journal of Computer Science and Cybernetics. Recently, Dr. Son has been

appointed as Consultant of Vietnam Government Office. So far, he has awarded "2014 VNU Research Award for Young Scientists", "2015 VNU Annual Research Award", "2015 Vietnamese Mathematical Award", and "2017 Vietnamese Mathematical Award".

Raghvendra Kumar is working as Assistant Professor in Computer Science and Engineering Department at L.N.C.T Group of College Jabalpur, M.P. India. He received B. Tech. in Computer Science and Engineering from SRM University Chennai (Tamil Nadu), India, M. Tech. in Computer Science and Engineering from KIIT University, Bhubaneswar, (Odisha) India and Ph.D. in Computer Science and Engineering from Jodhpur National University, Jodhpur (Rajasthan), India. He has published 86 research papers in international / National journal and conferences including IEEE, Springer and ACM as well as serve as session chair, Co-chair, Technical program Committee members in many international and national conferences and serve as guest editors in many special issues from reputed journals (Indexed By: Scopus, ESCI). He also received best paper award in IEEE Conference 2013 and Young Achiever Award-2016 by IEAE Association for his research work in the field of distributed database. His researches areas are Computer Networks, Data Mining, cloud computing and Secure Multiparty Computations, Theory of Computer Science and Design of Algorithms. He authored 12 computer science books in field of Data Mining, Robotics, Graph Theory, and Turing Machine by IGI Global Publication, USA, IOS Press Netherland, Lambert Publication, Scholar Press, Kataria Publication, Narosa, Edupedia Publication, S. Chand Publication and Laxmi Publication.

Sudan Jha was born on October 22 at the Capital city Kathmandu of Himalayan Country Nepal, he received proficiency in certificate level from Saint Xavier's College Kathmandu and then Bachelor of Engineering in Electronics Engineering from Motilal Nehru Regional College, Allahabad. Uttar Pradesh, India, in 2001; joined as a Lecturer in one of the premium and largest Engineering College and the first one in the private domain in Nepal ("Nepal Engineering College (nec)"), where he got full sponsorship from the employer (nec) to pursue "Masters in Computer Science". In due course of time, he chaired and organized 5 International Conferences, some of the proceedings of those conferences been published by Springer Verlag, World Science Series, Imperial Press London, etc. He was promoted to Assistant Professor in the Department of Computer Science and Engineering after completion of his Masters Degree and no sooner than later, he became the Head of the Computer Science and Engineering Department.

Affiliations

Rajiv Kapoor [1] · Rashmi Gupta [2] · Le Hoang Son [3,4] · Raghvendra Kumar [5] · Sudan Jha [6]

> Rajiv Kapoor
> rajivkapoor@dce.ac.in

> Rashmi Gupta
> rashmig71@yahoo.com

> Raghvendra Kumar
> raghvendraagrawal7@gmail.com

> Sudan Jha
> jhasudan@hotmail.com

[1]   ECE Department, Delhi Technological University, Delhi, India

[2]   ECE Department, AIACT&R, GGSIPU, Delhi, India

[3]   Institute of Research and Development, Duy Tan University, Da Nang, Vietnam

[4]   VNU Information Technology Institute, Vietnam National University, Hanoi, Vietnam

[5]   Computer Science and Engineering Department, LNCT College, Bhopal, MP, India

[6]   School of Computer Engineering, Kalinga Institute of Industrial Technology, Bhubaneswar, Odisha, India